Programmable apodizer in incoherent imaging systems using a digital micromirror device

Chu-Ming Cheng
Jyh-Long Chern
National Chiao Tung University
Institute of Electro-Optical Engineering
Department of Photonics
Microelectronics and Information System Research Center
1001 University Road
Hsinchu, 300 Taiwan
E-mail: chuming.eo92g@nctu.edu.tw

Abstract. We propose a programmable apodizer using a digital micromirror device and the total-internal-reflection prism subsystem for incoherent imaging systems. It is shown that the proposed programmable apodizer can extend the depth of focus with the specific shaped aperture generated by the digital micromirror device. With a scale ratio of $K \leqslant 0.05$, one can achieve almost the same level of imaging quality as provided by the conventional annular apodizer, where K represents the ratio between the integer multiple of the micromirror's square pixel size and the diameter of the effective aperture stop. [DOI: 10.1117/1.3314306]

Subject terms: apodizer; optical transfer function; incoherent imaging system.

Paper 090331R received May 8, 2009; revised manuscript received Oct. 28, 2009; accepted for publication Dec. 18, 2009; published online Feb. 23, 2010.

1 Introduction

The current consumer applications of optical instruments and equipment demand high imaging quality, optical efficiency, and high resolution with the volume of the machine, nevertheless, being compact. At the same time, extending the depth of focus (EDOF) in an imaging system has been a long-standing issue in optical designs. Enhancing the quality of an image can be achieved and determined not only by the pupil function but also by its amplitude transmittance.[1] Nonuniform amplitude transmission filters can be employed to vary the response of an optical imaging system, for instance, to increase the focal depth and to decrease the influence of spherical aberration. Earlier EDOF investigations and experiments were carried out on annular apodizers,[2,3] the radial Walsh filter,[4] nonuniform-shaped apertures,[1,5] and wavefront coding[6,7] in imaging systems, where the nature of light is *incoherent*. However, none of those are programmable for the amplitude transmission at the aperture stop. From the point of view of potential applications as well as from a purely academic interest perspective, it is worthwhile to explore the possibility of how to realize a programmable apodizer for incoherent imaging systems.

In the literature, amplitude-transmitting filters for apodizing and hyperresolving can be implemented with a programmable liquid-crystal spatial light modulator operating in a transmission-only mode in a *coherent* imaging system with the laser light source, polarizers, and quarter-wavelength plates.[8,9] In this paper, we proposed a programmable apodizer using the digital micromirror device (DMD™; Texas Instrument, Dallas, Texas)[10] and the total-internal-reflection (TIR) prism subsystem in a polarization-free mode in an *incoherent* imaging system. We evaluated the imaging properties of the incoherent imaging system with a specific shaped aperture generated by DMD by calculating the optical transfer function (OTF) using the Hopkins method.[11] We also included the OTF of the specific shaped aperture for the conventional annular apodizer, which has been demonstrated, both theoretically and experimentally, by Mino and Okano[1] to show that the proposed programmable apodizer can not only extend the depth of focus but can also achieve almost the same level of imaging quality as the conventional annular apodizer in an incoherent imaging system.

The remainder of this paper is organized as follows. In Section 2, the configuration of the proposed system, which consists of a DMD and a TIR prism subsystem is illustrated. In Section 3, we derive the pupil functions of the differently shaped apertures, which are generated by the DMD. Then, in Section 4, we calculate the OTF in such an incoherent imaging system. Furthermore, the corresponding OTF is evaluated and then to identify the imaging performance for a system of perfect imaging (aberration free) as well as the defocused one in Section 5. Finally, the conclusions are given in Section 6.

2 Configuration of Optical System

The schematic sketch of an incoherent imaging system using one DMD and a charge-coupled device (CCD) imager is illustrated in Fig. 1. The system is formed by an image-taking lens module and a prism module. By following the paths of the axial rays as indicated by the solid lines in Fig.

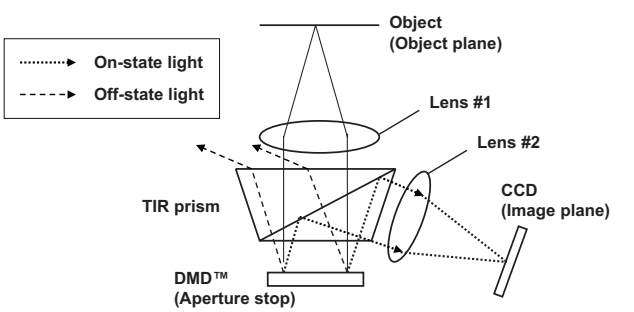

Fig. 1 Schematic diagram of the incoherent imaging system with the DMD and the TIR prism subsystem.

0091-3286/2010/$25.00 © 2010 SPIE

1, the rays starting from a point in the object pass through lens 1 and a prism module. The size of the axial cone of energy from the object is limited by the aperture stop on the DMD. The DMD consists of hundreds of thousands of moving micromirrors that are made to rotate to either +12 or −12 opositions depending on the binary state, i.e., on-state or off-state, of the underlying complementary metal oxide semiconductor synchronized dynamic random access memory cells below each micromirror.[10]

The DMD array size is 1024×768, and the pixel micromirrors measure $\sim 13.7\ \mu m^2$ to form a matrix having a high fill factor of $\sim 90\%$. The prism system comprises two transparent prisms, with an air gap between them. TIR at the interface between the prism and the air gap is utilized to separate the rays by their angle. The TIR prism has been applied into the DMD-based projection display in practice.[12] The prism system can guide the rays onto and away from the DMD, simultaneously. The rays indicated by the dotted lines in Fig. 1 from the object are imaged and focused onto the CCD by lens 2 when the configuration of the DMD is the on state. When the configuration of the DMD is the offstate, the rays indicated by the dashed lines in Fig. 1 are steered away in the opposite direction and the rays from the object are not imaged on the CCD. The DMD performs a spatial light modulation to rapidly generate a specific shaped aperture with either uniform or nonuniform illumination distribution at the aperture stop in an imaging system within the limited exposure time. This digital micromirror device can provide a programmable apodizer with a specific binary transmission for the incoherent imaging system. This implementation is not limited by this practical device. The TIR prism performs light separation to manage the illuminations and also make the normal vectors of the object, aperture stop, and image planes, respectively, coincide with the optical axis of the optical imaging system with the most compact volume.

3 Calculation of Pupil Functions

The pupil function of a defocused optical system with a circular symmetrical aperture is given by[1]

$$f(x,y) = T'(x,y)\exp[ik\omega_{20}(x^2+y^2)] \quad x^2+y^2 \leqslant 1$$

$$=0 \quad x^2+y^2 > 1, \tag{1}$$

where ω_{20} is the wave aberration of the defocused coefficient, (x,y) are the normalized Cartesian coordinates, and $k=2\pi/\lambda$, where λ is the wavelength of the light. Function $T'(x,y)$ in Eq. (1) represents the binary amplitude distribution over the normalized pupil coordinate that is scaled and normalized to make the outer periphery the unit circle, $x^2+y^2 \leqslant 1$. The binary amplitude transmittance $T'(x,y)$ is generated by the DMD as shown in Fig. 2. We can derive the amplitude transmittance of the shaped aperture $T'(x,y)$ in an on-state configuration as follows:

$$T'(x,y) = E'(x,y) \otimes \sum_m \sum_n T(x,y)\,\delta\left(x - \frac{2mc}{D}\right)\delta\left(y - \frac{2nc}{D}\right) \tag{2}$$

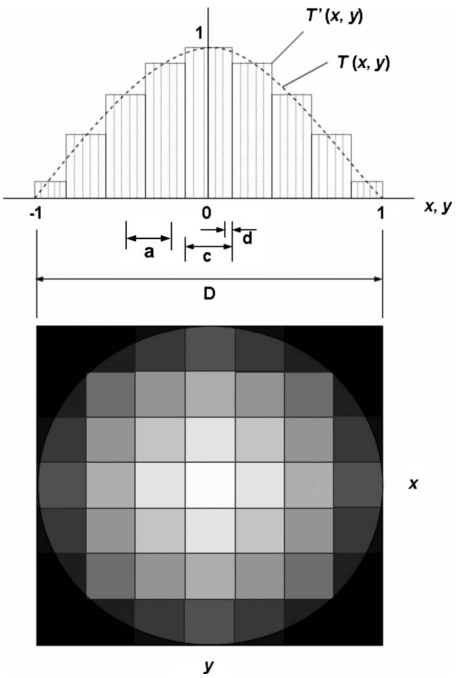

Fig. 2 Illustration of the binary amplitude transmittance $T'(x,y)$ for the normalized circular aperture, which is generated by the DMD. $T(x,y)$ represents a specifically shaped aperture for a conventional annular apodizer.

$$0 \leqslant |m|,|n| \leqslant \mathrm{Int}\left[\frac{D/c-1}{2}\right], \tag{3}$$

where $\otimes$ represents the convolution operation. $T(x,y)=1-(x^2+y^2)$ denotes the amplitude transmittance with a continuous profile at the aperture stop which can extend the focal depth in the imaging system with a conventional annular apodizer.[1] D is the corresponding diameter of the effective aperture stop. c represents the width of each square individual aperture generated by DMD in the pupil plane, which is equal to an integer multiple of the value d, with d being the width of each square pixel in the DMD. $\delta[x-(2mc/D)]\delta[y-(2nc/D)]$ denotes the δ function, indicating the location of the individual aperture in the normalized coordinate on the aperture stop. $E'(x,y)=[H(x+c/D)-H(x-c/D)]\times[H(y+c/D)-H(y-c/D)]$ is the binary amplitude transmittance of the individual shaped aperture, which is then scaled and normalized into the pupil coordinate. $Int[(D/c-1)/2]$ is the interpart of $[(D/c-1)/2]$. $H(x+c/D)$, $H(x-c/D)$, and $H(y+c/D)$ and $H(y-c/D)$ are the step functions. It is evident that the total aperture function is formed by convolving the individual aperture function with an appropriate array of the δ function, each located at one of the coordinate origins $(x_m,y_n)=(2mc/D,2nc/D)$, where $m, n=\ldots-2,-1,0,1,2,\ldots$

The quality and location of the individual aperture on the pupil depends on the scale ratio defined as

$$K \equiv (c/D) \tag{4}$$

for the specific diameter of the effective aperture stop on the DMD in the imaging system. The value of the scale

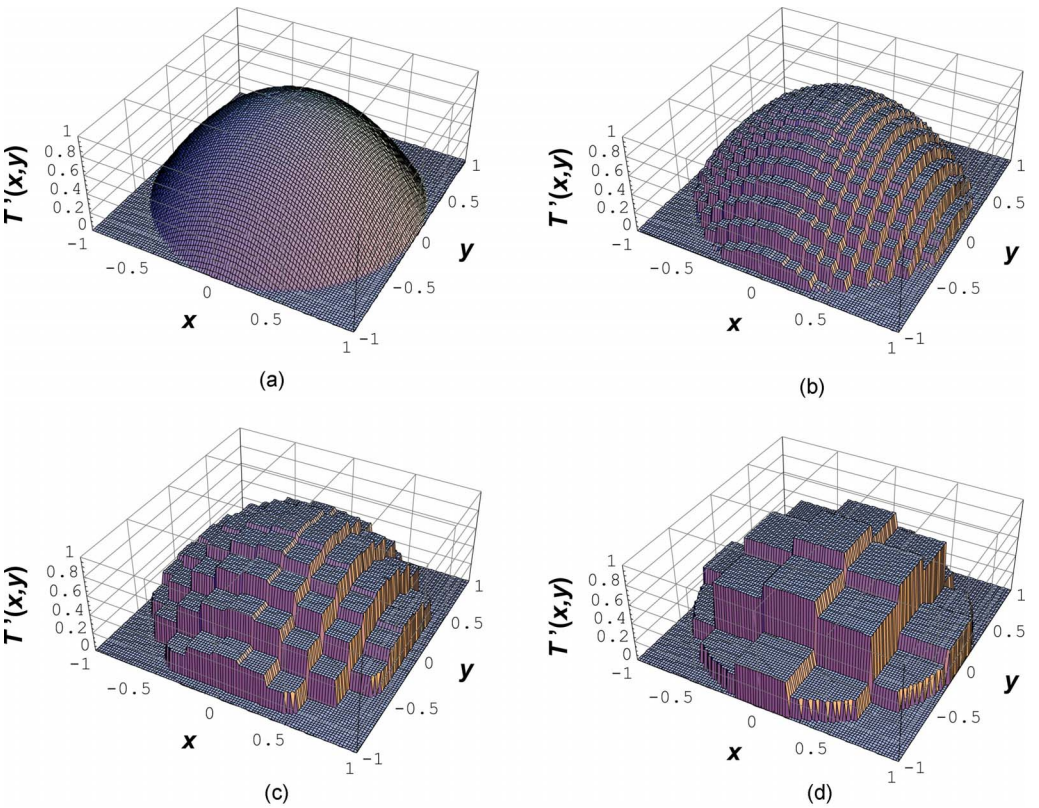

Fig. 3 Binary amplitude transmittance $T'(x,y)$ with $T(x,y)=1-(x^2+y^2)$ on the normalized pupil in the condition of $D=2$, and scale ratios at (a) $K=0$, (b) $K=0.05$, (c) $K=0.1$, and (d) $K=0.3$, which are generated by DMD.

ratio K determinates how many resolutions, how many gray levels, and how fast the DMD can dynamically generate the shaped apertures within a specific exposure time.

It is worthwhile to give an example for illustration. If the DMD array is 1024×768 with a pixel size of 13.7 μm^2, and the active area is 14.03×10.52 mm$=147.60$ mm^2,[10] then the number of D is ~10.52 mm (i.e., equal to the width of the active area of the DMD) if the effective aperture stop is located on the circular area centered at the actual DMD. In the case of $K=0.05$, the width of each individual square aperture c is 0.53 mm and equivalent to 38 square pixels with the same amplitude transmittance. There are 10 (i.e., $Int[(D/c-1)/2]+1$) gray levels for a specific shaped aperture, including the full bright mode and full dark mode. The current DMD-based system can offer 8 bits or 256 gray levels within a time period of 5.6 ms per primary color.[10] Thus, the DMD can rapidly generate one shaped aperture with 10 gray levels within the very short exposure time of 0.22 ms (i.e., $5.6\times10/256$) in the case of $K=0.05$.

The computer program for evaluating Eqs. (2)–(4) is written in Mathematica software.[13] We assumed $D=2$ for the simplification and evaluated four cases for the scale ratios $K=0$, $K=0.05$, $K=0.1$, and $K=0.3$. The binary amplitude transmittances of the shaped apertures $T'(x,y)$ are shown in Fig. 3. The scale ratio $K=0$ stands for the amplitude transmittance with a continuous profile. It is evident that the scale level of the binary amplitude transmission at the aperture stop increases with the reduction of scale ratio K, and the distribution of the binary amplitude transmission gets close to the continuous profile if the scale ratio K decreases.

In order to evaluate the relationship between the image performance and the size of the individual square aperture on the normalized pupil, we modified Eqs. (2) and (3) to the following:

$$T'(x,y)=E'(x,y)\otimes\sum_m\sum_n T(x,y)\,\delta\left(x-\frac{2ma}{D}\right)\delta\left(y-\frac{2na}{D}\right), \tag{5}$$

$$0\leq|m|,|n|\leq\mathrm{Int}\left[\frac{D/a-1}{2}\right]+1, \tag{6}$$

where $\otimes$ represents the convolution operation. $T(x,y)=1$ denotes the amplitude transmittance with a clear aperture. D is the corresponding diameter of the effective aperture stop. c represents the width of each square individual aperture generated by DMD in the pupil plane. The parameter a represents the distance between each square individual aperture as shown in Fig. 2. $\delta[x-(2ma/D)]\delta[y-(2na/D)]$ denotes the δ function, indicating the location of the individual aperture in the normalized coordinate on the aperture stop. $E'(x,y)=[H(x+c/D)-H(x-c/D)]\times[H(y+c/D)-H(y-c/D)]$ is the binary amplitude transmittance of the individual shaped aperture, which is then scaled and nor-

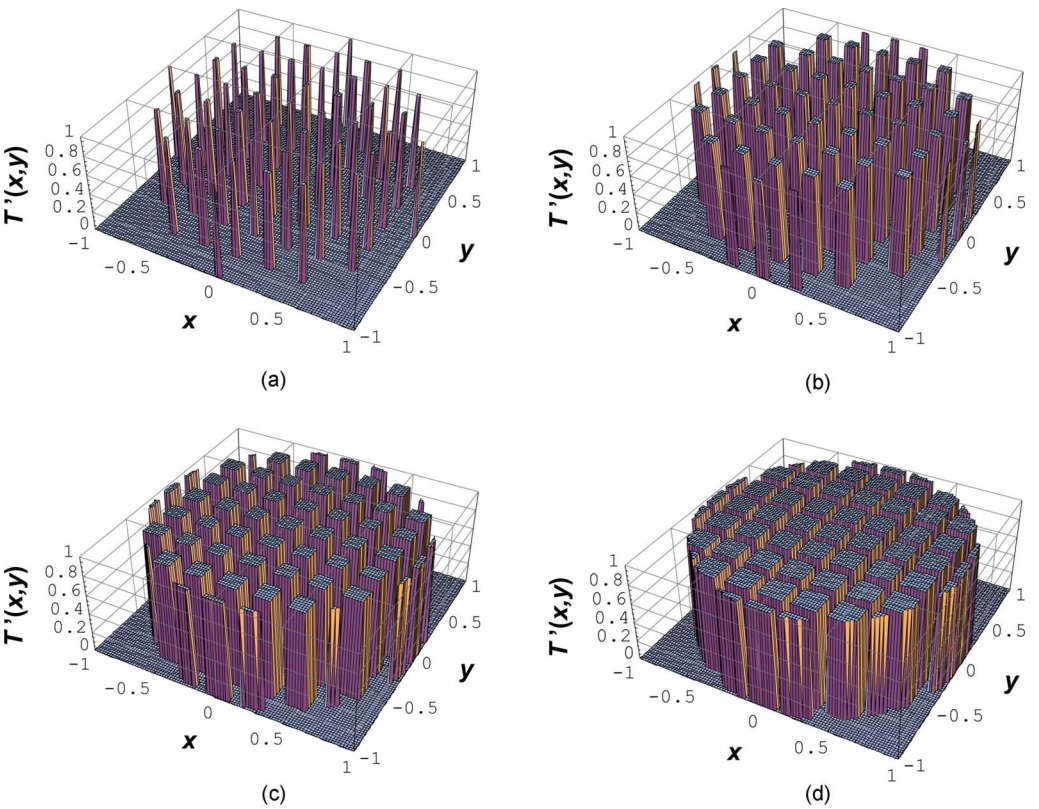

Fig. 4 Binary amplitude transmittance $T'(x,y)$ with $T(x,y)=1$ on the normalized pupil in the condition of $D=2$ and $a=0.25$ in different conditions of (a) $c=0.05$, (b) $c=0.1$, (c) $c=0.15$, and (d) $c=0.2$, which are generated by DMD.

malized into the pupil coordinate. $Int[(D/a-1)/2]$ is the interpart of $[(D/a-1)/2]$. $H(x+c/D)$, $H(x-c/D)$, $H(y+c/D)$, and $H(y-c/D)$ are the step functions. It is evident that the total aperture function is formed by convolving the individual aperture function with an appropriate array of the δ function, each located at one of the coordinate origins $(x_m,y_n)=(2ma/D,2na/D)$, where m, $n=\ldots-2,-1,0,1,2,\ldots$ We assumed $D=2$ and $a=0.25$ in Eqs. (5) and (6). Four cases of the binary amplitude transmittances $T'(x,y)$ for $c=0.05$, $c=0.1$, $c=0.15$, and $c=0.2$ were computed and shown in Fig. 4. There are nine individual apertures along the x- and y-axes within the pupil, respectively. The results show that the individual aperture size on the normalized pupil is shrunk with the width of each square individual aperture (i.e., the value c) generated by DMD. That is equivalent to the term $E\prime(x,y)$ varied with c in Eq. (5).

4 Optical Transfer Function of the Pupil with DMD

The OTF is derived from the autocorrelation of the pupil function by using the Hopkins canonical coordinate[11] and is given by

$$\tau(s)=\frac{g(s,0)}{g(0,0)}=\frac{\int_{-\infty}^{\infty}\int_{-\infty}^{\infty}f(x+s/2,y)f^*(x-s/2,y)dxdy}{\int_{-\infty}^{\infty}\int_{-\infty}^{\infty}f(x,y)f^*(x,y)dxdy}, \quad (7)$$

where $f(x,y)$ is the pupil function shown in Eq. (1), $f^*(x,y)$ is the complex conjugate of $f(x,y)$, and s is defined as the spatial frequency $s\equiv 2F\lambda N$. Here, F is the f-number of the imaging lens system, λ is the wavelength, and N is the number of cycles per unit length in the image plane. The denominator of Eq. (7) is the normalizing factor for making $\tau_0(0)=1$. The $g(s,0)$ and $g(0,0)$ in the OTF for the pupil function $f(x,y)$ can then be given by

$$g(s,0)=\int_{-[1-(s/2)^2]^{1/2}}^{[1-(s/2)^2]^{1/2}}\int_{-[(1-y^2)^{1/2}-s/2]}^{[(1-y^2)^{1/2}-s/2]}T'\left(x+\frac{s}{2},y\right)\cdot T'\left(x-\frac{s}{2},y\right)\exp[iAx]dxdy \quad (8)$$

and

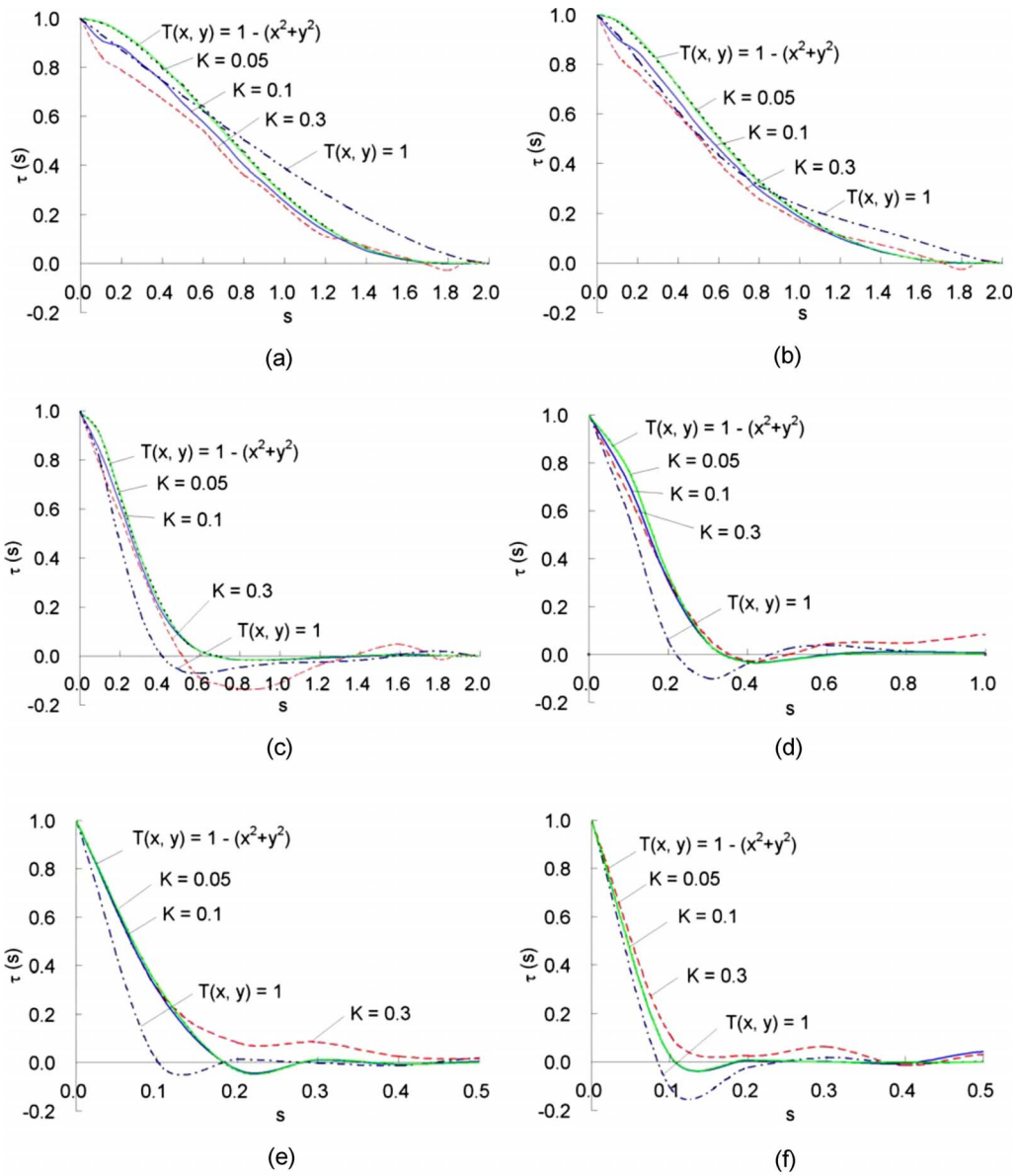

Fig. 5 Optical transfer functions in an aberration-free system and a defocused system with different defocused coefficients (a) $\omega_{20}=0$, (b) $\omega_{20}=\lambda/\pi$, (c) $\omega_{20}=3\lambda/\pi$, (d) $\omega_{20}=5\lambda/\pi$, (e) $\omega_{20}=10\lambda/\pi$, and (f) $\omega_{20}=15\lambda/\pi$, for binary amplitude transmittances of the aperture functions for $K=0.05$, $K=0.1$, and $K=0.3$, which are generated by the DMD, and for a clear aperture $T(x,y)=1$ and one specific shaped aperture $T(x,y)=1-(x^2+y^2)$ of a conventional annular apodizer, respectively.

$$g(0,0)=\int_{-1}^{1}\int_{-(1-y^2)^{1/2}}^{(1-y^2)^{1/2}}[T'(x,y)]^2dxdy, \tag{9}$$

where $A=2k\omega_{20}s$. Because the pupil function is an even function, the term of $\exp(iAx)$ can be reduced to $\cos[Ax]$ in the integral of Eq. (8). Then, $g(s,0)$ can be rewritten as

$$g(s,0)=\int_{-[1-(s/2)^2]^{1/2}}^{[1-(s/2)^2]^{1/2}}\int_{-[(1-y^2)^{1/2}-s/2]}^{[(1-y^2)^{1/2}-s/2]}T'\left(x+\frac{s}{2},y\right)\cdot T'\left(x-\frac{s}{2},y\right)\cos(Ax)dxdy. \tag{10}$$

Equations (9) and (10) can be further modified as

$$g(0,0)=\sum_{q=-p}^{p}\left\{\int_{-(1-y^2)^{1/2}}^{(1-y^2)^{1/2}}[T'(x,y)]^2dx\right\}\cdot\Delta y, \tag{11}$$

where $y=(1/p)\times q, \Delta y=(1/p)$.

$$g(s,0)=\sum_{q'=-p'}^{p'}\left\{\int_{-[(1-y^2)^{1/2}-s/2]}^{[(1-y^2)^{1/2}-s/2]}T'\left(x+\frac{s}{2},y\right)\cdot T'\left(x-\frac{s}{2},y\right)\cos(Ax)dx\right\}\cdot\Delta y, \tag{12}$$

where $y=[1-(s/2)^2]^{1/2}/p'\times q', \Delta y=[1-(s/2)^2]^{1/2}/p'$. By replacing the integral in Eqs. (9) and (10) with the y-axis

for the summation in Eqs. (11) and (12), an initial setting of $p=100$ is made for the number of intervals used to find the value of $\Delta y=[1-(s/2)^2]^{1/2}/p'$ and $\Delta y=1/p$ for $g(s,0)$ and $g(0,0)$, respectively. Different numbers of y, from $-[1-(s/2)^2]^{1/2}$ to $[1-(s/2)^2]^{1/2}$, are then used to calculate the OTF.

5 Imaging Performance Evaluation

The OTF of the different pupil functions are numerically computed using Mathematica software[13] based on Eqs. (1)–(4), (11), and (12) for binary amplitude transmittances of the aperture functions for $K=0.05$, $K=0.1$, and $K=0.3$, which are shown in Fig. 3. The OTF of the aberration-free and defocused system with a clear aperture $T(x,y)=1$ (i.e., a uniform-shaped aperture) and one specific shaped aperture $T(x,y)=1-(x^2+y^2)$, as $x^2+y^2\leqq 1$, and $T(x,y)=0$ as $x^2+y^2>1$, over the normalized pupil coordinate, which is scaled to make the outer periphery as one unit circle, i.e., $x^2+y^2\leq 1$, respectively, already investigated theoretically and experimentally in the literature,[1] are calculated again here for comparison.

The results for the aberration-free system (i.e., $\omega_{20}=0$) is shown in Fig. 5(a), and the defocused systems with $\omega_{20}=\lambda/\pi$, $3\lambda/\pi$, $5\lambda/\pi$, $10\lambda/\pi$, and $15\lambda/\pi$ are shown in Figs. 5(b)–5(f), respectively. We compared the OTF of the different scale ratios K to the OTF of a clear aperture $T(x,y)=1$. For the large values of ω_{20} [e.g., $5\lambda/\pi$, $10\lambda/\pi$, and $15\lambda/\pi$ as shown in Fig. 5(d)–5(f)], the spatial frequency corresponding to the first zero becomes smaller. Because the spatial frequency of the first zero generally represents the resolution limit of a defocused imaging system, we can take the first zero as defining the degree of focus. The larger degree of focus in the larger value of ω_{20} commonly represents the longer depth of focus in a defocused system. For the large values of ω_{20}, the degree of focus for the aperture with scale ratio $K<0.3$ is larger than for the aperture $T(x,y)=1$. It is evident that the specific shaped aperture, which is generated by the DMD with scale ratio $K=0.3$ or less, can then extend the depth of focus compared to a clear aperture in the conventional imaging system. We also compared the OTF of the different scale ratios K to the OTF of one specific shaped aperture $T(x,y)=1-(x^2+y^2)$. The OTF value of the former increased and got close to the OTF value of the latter when the scale ratio K decreased gradually, especially in the low spatial frequency region. This shows that the OTFs of the specifically shaped aperture, which are generated by the DMD, with scale ratio $K=0.05$ or less, can coincide with the OTF of the conventional annular apodizer with continuously shaped aperture.

To highlight the capability of our approach, we take a spoke pattern to explore imaging performance. Referring to Fig. 6, in column A, one could see the images for the clear aperture, while in column B, the images for the specific shaped aperture with scale ratio $K=0.05$ are shown. Furthermore, Figs. 6(a)–6(d) correspond to the images obtained with the defocused coefficients of $\omega_{20}=0$, $\omega_{20}=20\lambda/\pi$, $\omega_{20}=10\lambda/\pi$, and $\omega_{20}=15\lambda/\pi$ respectively. Comparing to the images for the specific shaped aperture, the images for the clear aperture show a more critical loss of contrast at high spatial frequencies with larger ω_{20}. Hence, we can conclude that the image quality will be enhanced as

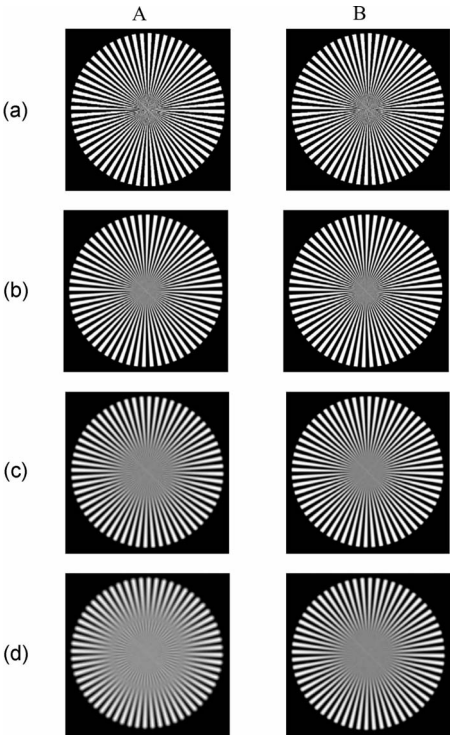

Fig. 6 The computer-simulated images of spoke patterns for (A) a clear aperture and (B) a specific shaped aperture with the scale ratio $K=0.05$ obtained with different defocused coefficients: (a) $\omega_{20}=0$, (b) $\omega_{20}=5\lambda/\pi$, (c) $\omega_{20}=10\lambda/\pi$, and (d) $\omega_{20}=15\lambda/\pi$.

the specific shaped aperture is used, especially for the large defocus coefficients in an imaging system. In other words, as for a real implementation of the DMD, the specific shaped aperture can extend the depth of focus compared to a clear aperture in the conventional imaging system.

In order to evaluate the relationship between the image performance and the size of the individual square aperture on the normalized pupil, we computed the OTF of the other types of pupil functions based on Eqs. (1), (5), (11), and (12) for the binary amplitude transmittances $T'(x,y)$ for $c=0.05$, $c=0.1$, $c=0.15$, and $c=0.2$ in the conditions of $T(x,y)=1$, $D=2$ and $a=0.25$, which is shown in Fig. 4. The OTF of the aberration-free system with a clear aperture $T(x,y)=1$ was also calculated here for comparison. The OTF's calculation results for the aberration-free system are shown in Fig. 7. The general tendency of the OTF curve versus the number of the individual aperture within the pupil is readily evident. There are nine individual apertures along x- and y-axes within the pupil, respectively. Meanwhile, there are nine peaks on the OTF curve at the near-periodic spatial frequencies around 0, 0.25, 0.50, 0.75, 1.00, 1.25, 1.50, 1.70, and 1.90. The OTF values of the odd-peak frequencies for different sizes of the individual apertures (i.e., value c) remain very similar to the values of the OTFs of the corresponding frequencies for the clear aperture. However, the OTF values of the even-peak frequencies can decrease with decrease in the size of the individual aperture. Therefore, if the size of an individual aperture is much less than that of pupil, then OTF values of the even-peak frequencies will almost be zero.

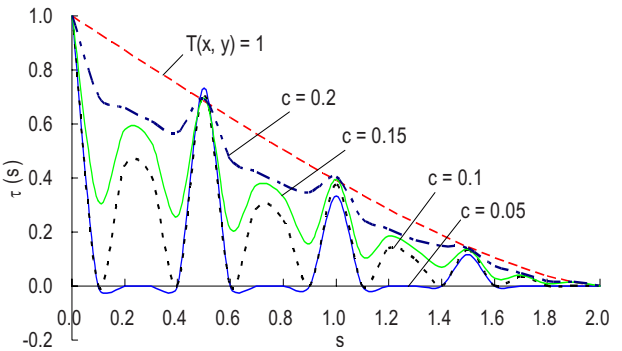

Fig. 7 Optical transfer functions in an aberration-free system with a clear aperture and the binary amplitude transmittances of the aperture functions for different conditions of c=0.05, c=0.1, c=0.15, and c=0.2, which are generated by the DMD.

6 Conclusions

One programmable apodizer using the DMD and TIR prism system has been applied to incoherent imaging systems. The OTF model semianalytically demonstrated that the proposed programmable apodizer for the specifically shaped aperture generated by a DMD can extend the depth of focus compared to a clear aperture in a defocused system. It shows that the specifically shaped aperture with scale ratio of $K \leqslant 0.05$ can achieve the same improved imaging quality as that of the conventional annular apodizer. Meanwhile, the general tendency of the OTF curve versus the number of the individual aperture and the binary amplitude transmittances with the discontinuous peak profile within the pupil has been investigated. It is evident that the OTF values of the even-peak frequencies can decrease when the size of the individual aperture decreases.

It is worth noting that the proposed model can rapidly generate one specifically shaped aperture with 10 gray levels within the very short exposure time of 0.22 ms in the case of K=0.05. On the other hand, the TIR prism can make the normal vectors of the object, aperture stop and image planes, respectively, coincide with the optical axis of the optical imaging system for a very compact volume. Further refinement of the shaped aperture design should be able to dynamically provide improved imaging quality for many varied scenes.

Acknowledgments

This work was supported in part by the National Science Council of Taiwan R.O.C. under Project No. 93-2215-E-009-057, and in part by the Ministry of Education and the Academic Top University program at the National Chiao Tung University, Taiwan.

References

1. M. Mino and Y. Okano, "Improvement in the OTF of a defocused optical system through the use of shaded apertures," *Appl. Opt.* **10**, 2219–2225 (1971).
2. J. Ojeda-Castaneda, P. Andrea, and A. Diaz, "Annular apodizers for low sensitivity to defocus and to spherical aberration," *Opt. Lett.* **11**, 487–489 (1986).
3. J. Ojeda-Castaneda, L. R. Berriel-Valdos, and E. L. Montes, "Bessel annular apodizers: imaging characteristics," *Appl. Opt.* **26**, 2770–2772 (1987).
4. L. N. Hazra and A. Guha, "Far-field diffraction properties of radial Walsh filters," *J. Opt. Soc. Am. A* **3**, 843–846 (1986).
5. C. S. Chung and H. H. Hopkins, "Influence of nonuniform amplitude on the optical transfer function," *Appl. Opt.* **28**, 1244–1250 (1989).
6. E. R. Dowski Jr. and W. T. Cathey, "Extended depth of field through wave-front coding," *Appl. Opt.* **34**, 1859–1866 (1995).
7. J. van der Gracht, E. R. Dowski, M. G. Taylor, and D. M. Deaver, "Broadband behavior of an optical-digital focus-invariant system," *Opt. Lett.* **21**, 919–921 (1996).
8. J. A. Davis, J. C. Escalera, J. Campos, A. Marquez, and M. J. Yzuel, "Programmable axial apodizing and hyperresolving amplitude filters with a liquid-crystal spatial light modulator," *Opt. Lett.* **24**, 628–630 (1999).
9. A. Marquez, C. Iemmi, J. Campos, J. C. Escalera, and M. J. Yzuel, "Programmable apodizer to compensate chromatic aberration effects using a liquid-crystal spatial light modulator," *Opt. Express* **13**, 716–730 (2005).
10. D. Dudley, W. Duncan, and J. Slaughter, "Emerging digital micromirror device (DMD) application," *Proc. SPIE* **4985**, 14–15 (2003).
11. H. H. Hopkins, "The Frequency Response of a Defocused Optical system," *Proc. R. Soc., London* **231**, 91–103 (1955).
12. C. M. Cheng and J.-L. Chern, "Design of a dual-F-number illumination system and its application to projection display with DMD™," *J. Soc. Inf. Disp.* **14**, 819–827 (2006).
13. Mathematica, version 4, Wolfram Research, Inc., Champaign, IL.

Chu-Ming Cheng received his BS in physics from National Sun Yat-sen University in 1995 and MS in electro-optical engineering from National Chiao Tung University in 1997, where he is currently a PhD student in electro-optical engineering. Cheng is also an R&D director in the light-engine R&D Department in Young Optics Inc. He has mainly worked on the design and development of the optical systems in DMD-based projection display technologies for 11 years, and has the 40 issued patents.

Jyh-Long Chern received his BS and MS in physics from the National Tsing Hua University, Hsinchu, Taiwan, in 1984 and 1986, respectively. He received his PhD in optical science from the University of New Mexico, Albuquerque, in 1991. He was a postdoctoral fellow at the Basic Research Laboratories, Nippon Telegram and Telephone Corporation, Japan, from April 1991 to August 1992. After his postdoctoral career, he joined the National Sun Yat-sen University, Kaohsiung, Taiwan, in 1992, as an associate professor of physics. In 1995, he became a full professor, and in 1996, he moved to the National Cheng Kung University, Tainan, Taiwan, as a full professor of physics. In August 2002, He joined the faculty of National Chiao-Tung University, where he is currently a professor of electro-optical engineering.